Effects of temperature and strain rate on tensile properties and activation energy for dynamic strain aging in alloy 625

Article *in* Metallurgical and Materials Transactions A · October 2004

DOI: 10.1007/s11661-004-0057-0

CITATIONS
53

READS
230

4 authors, including:

Vani Shankar
Indira Gandhi Centre for Atomic Research
46 PUBLICATIONS **593** CITATIONS
SEE PROFILE

M. Valsan
Indira Gandhi Centre for Atomic Research
29 PUBLICATIONS **285** CITATIONS
SEE PROFILE

Kota bhanu sankara rao
Mahatma Gandhi Institute of Technology
252 PUBLICATIONS **3,408** CITATIONS
SEE PROFILE

Effects of Temperature and Strain Rate on Tensile Properties and Activation Energy for Dynamic Strain Aging in Alloy 625

VANI SHANKAR, M. VALSAN, K. BHANU SANKARA RAO, and S.L. MANNAN

Alloy 625 ammonia cracker tubes were service exposed for 60,000 hours at 873 K. These were then subjected to a solution-annealing treatment at 1473 K for 0.5 hours. The effects of temperature and strain rate on the tensile properties of the solution-annealed alloy were examined in the temperature range of 300 to 1023 K, employing the strain rates in the range of $3 \times 10^{-5}\ s^{-1}$ to $3 \times 10^{-3}\ s^{-1}$. At intermediate temperatures (523 to 923 K), various manifestations of dynamic strain aging (DSA) such as serrated flow, peaks, and plateaus in the variations of yield strength (YS) and ultimate tensile strength (UTS) and work-hardening rate with temperature were observed. The activation energy for serrated flow (Q) was determined by employing various methodologies for $T < 823$ K, where a normal Portevien–Le Chatelier effect (PLE) was observed. The value of Q was found to be independent of the method employed. The average Q value of 98 kJ/mol was found to be in agreement with that for Mo migration in a Ni matrix. At elevated temperatures ($T \geq 823$ K), type-C serrations and an inverse PLE was noticed. The decrease in uniform elongation beyond 873 K for $3 \times 10^{-5}\ s^{-1}$ and $3 \times 10^{-3}\ s^{-1}$ and beyond 923 K for $3 \times 10^{-4}\ s^{-1}$ strain rates seen in this alloy has been ascribed to reduction in ductility due to precipitation of carbides and δ phase on the grain boundaries.

I. INTRODUCTION

ALLOY 625 is a wrought nickel-based superalloy strengthened by the solid-solution-hardening effects of chromium, molybdenum, niobium, and iron and precipitation-hardening effects of the intermetallic phases like bct γ'', orthorhombic δ, and Pt_2Mo-type $Ni_2(Cr, Mo)$.[1–9] The alloy has been developed for service at temperatures below 973 K, and it possesses high strength and excellent fabrication characteristics. The alloy is being used for a variety of components in aerospace, aeronautic, marine, chemical, petrochemical, and nuclear industries. It is also being used extensively in the form of tubes in ammonia cracker plants associated with heavy-water production. During normal service, the cracker tubes are exposed to a gas pressure of 14 MPa and temperatures in the range of 853 to 973 K. At these temperatures, the ammonia cracker tubes undergo creep deformation. Although the design life of the cracker tubes is 10^5 hours, some failures have taken place after about 60,000 hours of service, necessitating their premature replacement. Since replacement of all the tubes is very expensive, rejuvenation heat treatments have been suggested recently by Vani Shankar *et al.*[9,10] to regain partially the degraded properties. Complete rejuvenation of tensile properties through a solution-annealing treatment at 1423 K for 0.5 hours has been found to be beneficial with respect to tensile properties.[9,10,11]

Dynamic strain aging (DSA) is known to occur in austenitic stainless steels and Ni-Fe–based superalloys over a range of temperatures and strain rates.[11–14] Serrated flow, one of the manifestations of DSA,[15] has been observed in the temperature range of application of alloy 625 by the present authors. This may have a large impact on the mechanical properties and life of the cracker tubes.

The various investigations of serrated flow suggest that the measurement of ε_c, the critical strain for the onset/termination of serrations,[16] and its dependence on strain rate ($\dot{\varepsilon}$) and temperature (T) is essential to understand the underlying mechanisms. This dependence is generally expressed as

$$\varepsilon_C^{(m+\beta)} = K\dot{\varepsilon} \exp(Q/kT) \qquad [1]$$

where m and β are the respective exponents in the relations for the variation of vacancy concentration (C_v) and mobile dislocation density (ρ_m) with plastic strain ($C_v \propto \varepsilon^m$ and $\rho_m \propto \varepsilon^\beta$, respectively), K is a constant, Q is the activation energy, k is the Boltzman constant, and T is the absolute temperature.[17,18] One can obtain the exponent ($m + \beta$) as the slope in the plot of $\ln \dot{\varepsilon}$ *vs* $\ln \varepsilon_c$ at a constant temperature. There are several methods for evaluating Q associated with serrated flow, which are described as follows.

(1) Following Eq. [1], the slope of a plot of $\ln \varepsilon_c$ *vs* $1/T$ at constant $\dot{\varepsilon}$ can be used to evaluate Q as Q = slope $\times$ ($m + \beta$) $\times$ k. However, as pointed out by Qian and Reed- Hill,[19] this method involves the use of an average value of ($m + \beta$) obtained over a range of $\dot{\varepsilon}$ and T values.
(2) From the $\ln \dot{\varepsilon}$ *vs* $\ln \varepsilon_c$ plots, one can obtain intercepts on the $\ln \dot{\varepsilon}$ axis corresponding to different levels of critical strain at different temperatures. A replot of these intercept values of $\ln \dot{\varepsilon}$ *vs* $1/T$ corresponding to different critical strain levels will yield a set of parallel lines, whose average slope is related to Q as Q = slope $\times$ k.[19,20] It may be noted that this intercept method does not involve the use of ($m + \beta$).
(3) The quasistatic aging model[17] relates the concentration dependence of ε_c as

$$\varepsilon_C^{(m+\beta)}/T = \left(\frac{C_1}{\phi C_0}\right)^{3/2} \frac{k\mathbf{b}}{LNU_m} \frac{\exp(Q/kT)}{D_0} \dot{\varepsilon} \qquad [2]$$

VANI SHANKAR, Scientific Officer, Mechanical Metallurgy Division, M. VALSAN, Head, Fatigue Studies Section, Mechanical Metallurgy Division, K. BHANU SANKARA RAO, Head, Mechanical Metallurgy Division, and S.L. MANNAN, Associate Director, are with the Indira Gandhi Centre for Atomic Research, Kalpakkam-603 102, India. Contact e-mail: bhanu@igcar.ernet.in

Manuscript submitted May 30, 2003.

where C_0 is the initial concentration of solute in the alloy, C_1 is the local concentration of the solute at the dislocation, L is the obstacle spacing, U_m is the maximum solute-dislocation interaction energy, D_0 is the frequency factor, **b** is the Burger's vector, and N and ϕ are constants. Using the previous equation, Kim and Chaturvedi[21] have evaluated Q for a given $\dot{\varepsilon}$ value from the plot of $\ln \varepsilon_c{}^{(m+\beta)}/T$) *vs* $1/T$ as Q = slope × k. In this method, it would be possible to use the individual values of $(m + \beta)$ obtained at different temperatures.

(4) The value of Q can also be obtained from the load-drop measurements as suggested by Pink and Grinberg[22] based on Russell's approach.[23]

The aim of the present article is to (a) study the influence of strain rate and temperature on the tensile properties and serrated-flow behavior of service-exposed–plus–solution-annealed alloy 625, (b) evaluate the activation energy for DSA using methods 1 through 3 mentioned previously and identify the species responsible for DSA, and (c) correlate the observed mechanical properties with the fracture modes.

II. EXPERIMENTAL PROCEDURE

The current investigation has been conducted on alloy 625 tube retrieved from an ammonia cracker plant after 60,000 hours of service at approximately 873 K. The chemical composition (in wt pct) of the alloy investigated is as follows: Cr-21.7, Fe-3.9, Mo-8.8, Nb-3.9, C-0.05, Mn-0.14, Si-0.15, Al-0.17, Ti-0.23, Co-0.08, and the balance Ni.

Solution annealing at 1423 K for 0.5 hours was found to be adequate for dissolving all the chromium-rich carbides and intermetallic compounds (γ'' and Ni_2(Cr, Mo)) which had formed during the service exposure of the alloy. The mean grain size obtained after solution annealing was ~70 μm. The tube had a wall thickness of 9 mm and outer diameter of 90 mm. The blanks of 60 × 10 × 9 mm were cut from the solution-annealed tubes in the longitudinal direction, and button-head tensile-test specimens of 4 mm in diameter and 25 mm in gage length were fabricated. Tensile tests were carried out in air at different temperatures in the range of 300 to 1023 K and at strain rates varying from 3×10^{-5} s^{-1} to 3×10^{-3} s^{-1} using an Instron model 1195 universal testing machine. During the elevated-temperature tests, the specimen temperature was stabilized for 15 minutes prior to the commencement of testing. The engineering properties, such as 0.2 pct offset yield strength (YS), ultimate tensile strength (UTS), and uniform elongation were evaluated from the load-elongation charts. Fractography of the tensile-tested samples was carried out using a scanning electron microscope.

III. RESULTS

A. *Microstructural Investigations*

Transmission electron microscopy on the service-exposed alloy shows extensive intragranular and intergranular precipitation (Figure 1(a)). A magnified image of Figure 1(a), shown in Figure 1(b), demonstrates that some of the intragranular precipitates have a snowflake morphology (marked as A in Figure 1(b)) and others have a lens shape (marked as B in Figure 1(b)). Figure 1(c) shows the selected-area diffraction pattern taken from the matrix using the [001] zone axis. Figures 1(c) and (d) show that superlattice reflections occur at the {100}, {110}, {11/20}, and 1/3 {220} positions. The {100}, {110}, and {11/20} reflections arise from the γ'' precipitate, whereas 1/3 {220} reflections arise from Ni_2(Cr, Mo) phase, having a Pt_2Mo-type structure.[2] Further analysis revealed the lens-shaped precipitates to be γ'' (Ni_3(Nb, Al, Ti)) phase and the snowflake type precipitates to be Ni_2(Cr, Mo) phase. A continuous film of carbides at the grain boundaries could also be seen in Figure 1(a). Figure 2 shows a bright-field image of a service-exposed alloy that is solution annealed at 1423 K for 0.5 hours. The solution annealing caused the dissolution of most of the pre-existing precipitates in the service-exposed state. However, a few large primary NbC precipitates remained undissolved. The alloy also contained a large number of uniformly distributed dislocations that formed during the quenching operation.

B. *Serrated Flow and Activation Energy*

Load-elongation curves were obtained for the specimens tested in the temperature range of 300 to 1023 K at various strain rates in the range of 3×10^{-5} s^{-1} to 3×10^{-3} s^{-1}. At ambient temperature, load-elongation curves remained smooth irrespective of the strain rate employed. Serrations appeared on the load-elongation curves between 523 and 1023 K. The height of serrations was found to increase with progressive deformation, increase in temperature, and decrease in strain rate. The load-elongation segments for the various test temperatures at the lowest strain rate (3×10^{-5} s^{-1}) are shown in Figure 3. These curves describe the variation in the stress response under serrated yielding conditions at various temperatures. The starting stress and strain levels of the stress-strain segments presented are indicated in the figure. The different types of serrations are labeled following the generally accepted nomenclature in the literature.[13,18,23]

The general characteristics of various types of serrations are classified as follows. Type-A serrations are periodic serrations from repeated deformation bands initiating at the same end and propagating in the same direction. These are locking serrations characterized by an abrupt rise in stress followed by a drop to or below the general level of the stress-strain curve. Type-B serrations are oscillations about the general level of the stress-strain curve that occur in quick succession due to discontinuous band propagation arising from the DSA of moving dislocations within the Luders band. Type-C serrations are yield drops below the general level of the stress-strain curve due to unlocking of dislocations.

At the lowest strain rate, *i.e.,* 3×10^{-5} s^{-1}, type-(A + B) serrations were observed at 723 K and below (Figure 3(b)). At temperatures above 723 K, type-C serrations were observed (Figure 3(c)). At the intermediate strain rate, type-(A + B) serrations were observed up to 773 K, beyond which type-C serrations were seen. At the fastest strain rate, type-C serrations were observed at and above 873 K, below which type-(A + B) serrations were seen. The type-C serrations that occur at and above 923 K for a 3×10^{-5} s^{-1} strain rate became scarce with progressive deformation and generally disappeared at larger strains (Figure 3(a)). Similar observations were made at and above 923 K for a 3×10^{-4} s^{-1}

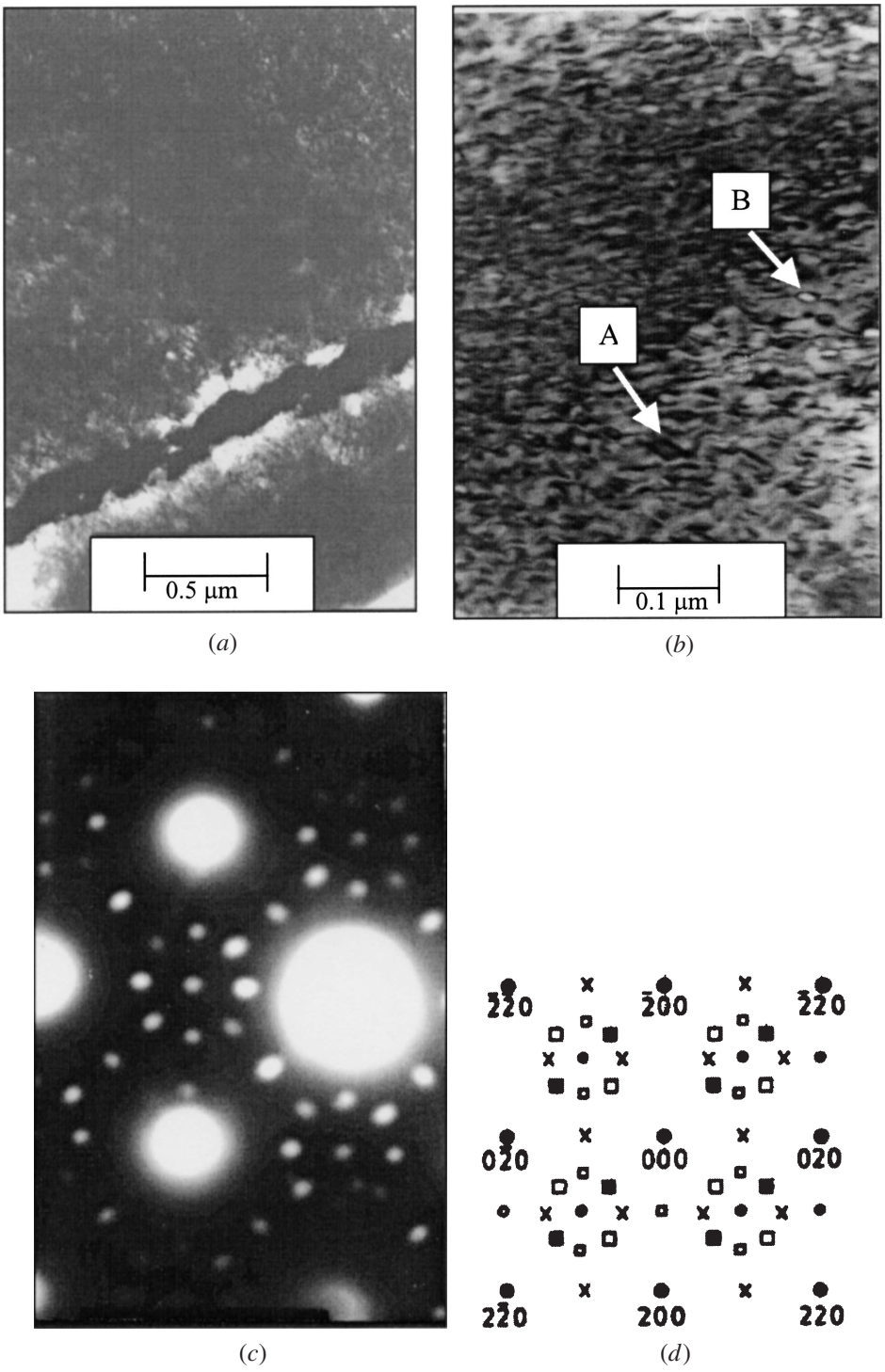

(*a*) (*b*) (*c*) (*d*)

Fig. 1—(*a*) Bright-field (BF) image of service-exposed alloy 625 showing extensive intragranular precipitation and grain boundary carbides. (*b*) Magnified image of (a) showing snowflaky (A) and lens (B) morphology of $Ni_2(Cr, Mo)$ and γ'' phases, respectively. (*c*) Selected area diffraction (SAD) image taken from matrix, using [001] zone axis showing superlattice reflections of both $Ni_2(Cr, Mo)$ and γ'' precipitates. (*d*) Key to diffraction pattern shown in (c); in this pattern, □ and ■ represent the two variants of the $Ni_2(Cr, Mo)$ phase and x, ● and □ represent the superlattice reflections corresponding to the [100], [010], and [001] variants of γ'' phase.

strain and at and above 973 K for a 3×10^{-3} s^{-1} strain. A summary of the observations made on the serrated-flow behavior is given in Figure 4.

The trend shown by type-C serrations at lower temperatures is different from that observed at higher temperatures. At 823 and 873 K and at the lowest strain rate, the small-amplitude type-C serrations, present initially, diminish after a few percentages of elongation. Later, comparatively large-amplitude regular type-C serrations occurred and continued through fracture. The behavior of serrations at 873 and 923 K for the intermediate and highest strain rates, respectively, were similar to those observed at 823 and 873 K at the lowest strain rate. Regular

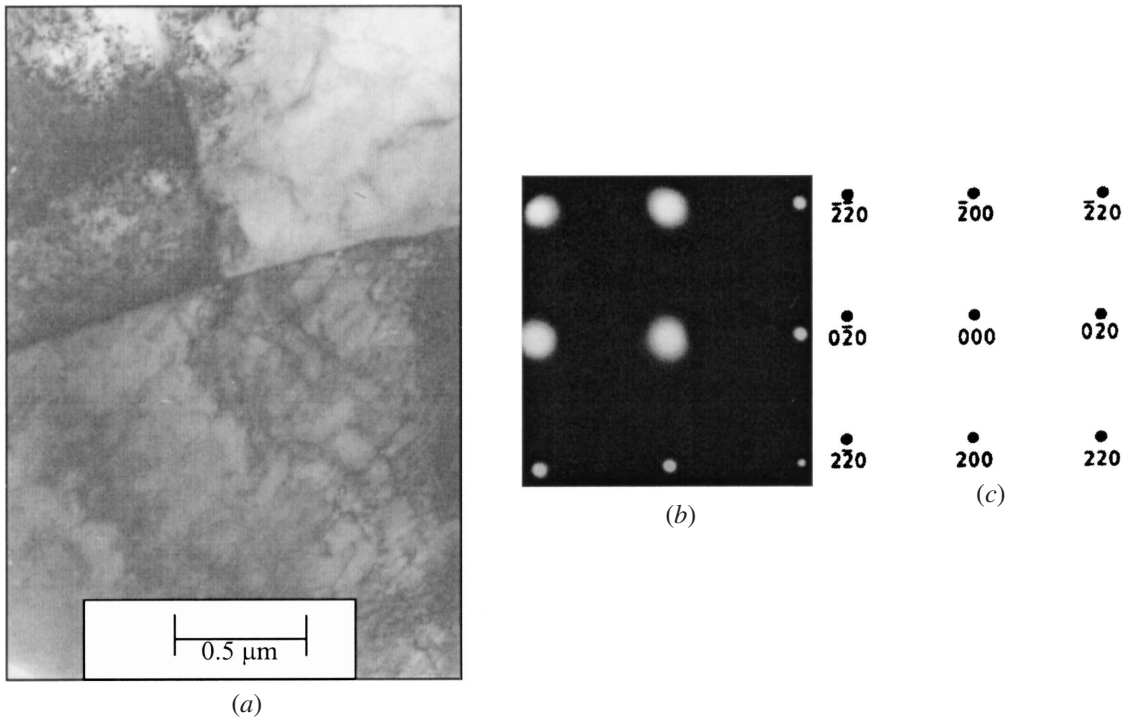

Fig. 2—(*a*) BF image of service-exposed alloy solution annealed at 1423 K for 0.5 h showing quenched-in dislocations. (*b*) SAD shows superlattice reflections of the matrix. (*c*) Key to diffraction pattern shown in (b).

type-C serrations were observed at 873 and 823 K for 3×10^{-3} s^{-1} and 3×10^{-4} s^{-1}, respectively.

Measurement of ε_c and its dependence on strain rate and temperature is essential to understand the underlying mechanism of DSA. The critical plastic strain (ε_c) is calculated from the load-elongation charts as the minimum value of true plastic strain at which a perceptible load drop of 5 N occurs. A systematic trend was noticed in the variation of critical strain with temperature and strain rate, as shown in Figure 5. For the onset of type-(A + B) serrations, ε_c decreased with increasing temperature at all the strain rates investigated up to 823 K. The value of ε_c for the onset of type-(A + B) serrations is greater at higher strain rates and decreases with increasing temperature, indicating the occurrence of the normal Portevin–Le Chatelier effect (PLE).

The values of Q determined from methods 1 through 3, as mentioned in the Introduction, along with $(m + \beta)$ values are listed in Table I. According to Eq. [1] $\left(\varepsilon_c^{(m+\beta)} = K\dot{\varepsilon} \exp(Q/kT)\right)$, the slopes of such plots directly yield the values of the exponent $(m + \beta)$. Using the average value of $(m + \beta)$ obtained from Figure 6(a), the activation energy is calculated from Figure 6(b), following method 1. The activation-energy value obtained using this method lies in the range of 81 to 125 kJ/mol. Similarly, the $(m + \beta)$ and Q values according to method 2 are computed from plots in Figures 7(a) and (b), respectively. The value of Q is computed according to the intercept method, *i.e.,* method 2, from a plot of ln $\dot{\varepsilon}$ *vs* $1/T$ (Figure 7(b)) for different strain levels, which is derived from Figure 7(a). Using method 2, the value of Q was found to be in the range of 93 to 106 kJ/mol. Finally, method 3 is employed for the determination of Q from the plot of ln $(\varepsilon_c^{(m+\beta)}/T)$ against $1/T$ (Figure 8). This gives a Q value in the range of 84 to 94 kJ/mol. Thus, the overall average value of Q obtained using the three aforementioned methods is 98 kJ/mol.

C. *Tensile Properties*

Variation of normalized tensile properties (normalized with the elastic modulus (E)), namely, normalized yield strength (YS/E), normalized ultimate tensile strength (UTS/E), uniform elongation, and normalized work-hardening rate (θ/E), where $\theta = (\sigma_{0.05}$ to $\sigma_{0.005})/0.045$, are shown in Figures 9(a) through (d), respectively, as a function of strain rate and temperature. The E values used in the present investigation at various temperatures are provided in Table II.[24] The YS decreases with increasing temperature up to 623 K and, thereafter, shows a gradual increase at all of the three strain rates investigated. The peaks in YS are shown at 923, 823, and 723 K for strain rates of 3×10^{-5} s^{-1}, 3×10^{-3} s^{-1}, and 3×10^{-4} s^{-1}, respectively (Figure 9(a)). The UTS also exhibits peaks at 873 K for 3×10^{-5} s^{-1} and 923 K for 3×10^{-4} s^{-1}, respectively (Figure 9(b)). Further, uniform elongation has a minimum at 623 K at strain rates of 3×10^{-5} s^{-1} and 3×10^{-3} s^{-1} (Figure 9(c)). It is also observed that beyond 923 K for 3×10^{-4} s^{-1}, both the UTS and uniform elongation decrease drastically with further increase in temperature. For 3×10^{-5} s^{-1}, the onset of the decrease in UTS and uniform elongation is observed around 873 K. Moreover, at 1023 K, both the UTS and uniform elongation decrease with decreasing strain rate (Figures 9(b) and (c)). It is observed from Figure 9(d) that the work-hardening rate increases initially with increasing temperature and exhibits double peaks for all the strain rates. These peaks are observed at 723 and 923 K for the highest strain rate, at 623 and 923 K for the intermediate strain rate, and at 623 and 823 K for the slowest strain rate.

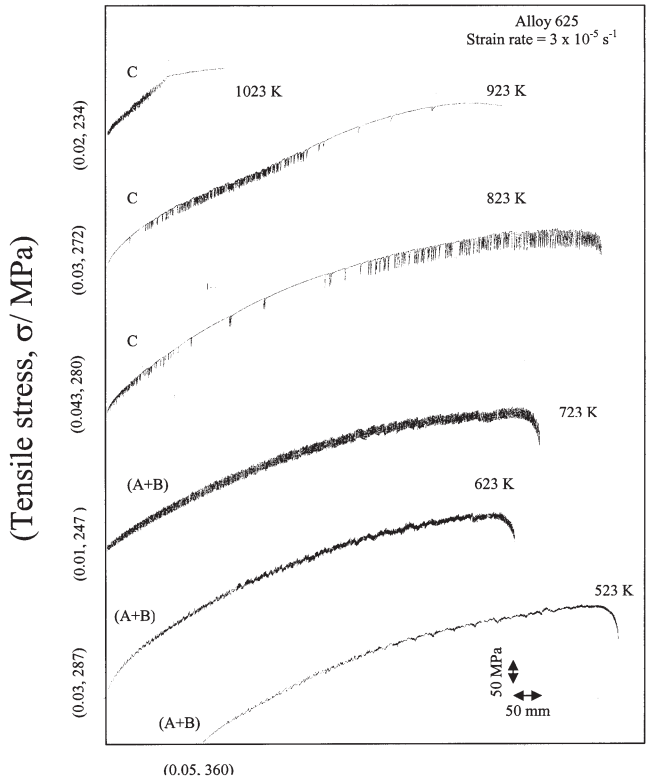

(*a*)

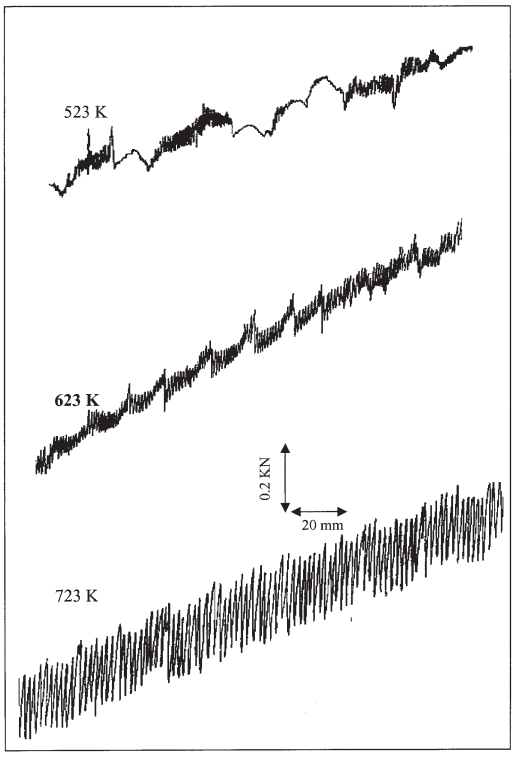

(*b*)

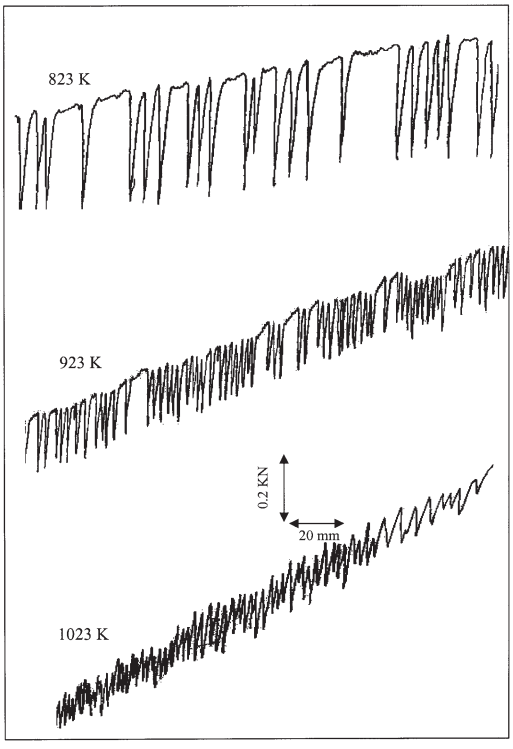

(*c*)

Fig. 3—(*a*) Load-elongation curves in alloy 625 at different temperatures; $\dot{\varepsilon} = 3 \times 10^{-5}\ s^{-1}$ depicting serrated flow. Values in parenthesis represent the starting value of the plastic strain and the corresponding stress value (MPa) of the load-elongation segment. (*b*) Magnified view of serrations observed in flow curves, $T \leq 723$ K. (*c*) Magnified view of serrations observed in flow curves, $T > 723$ K.

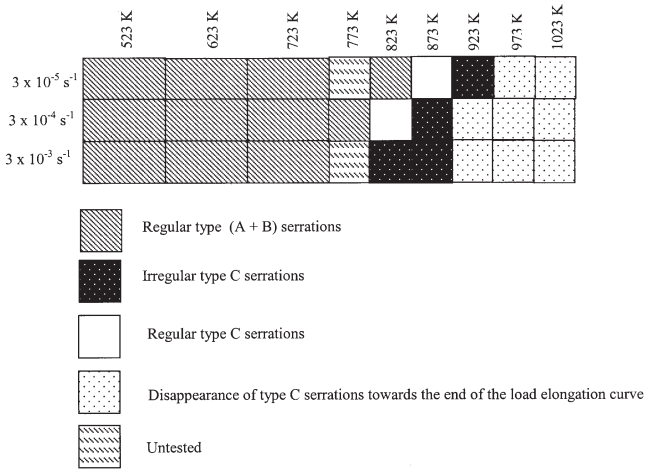

Fig. 4—Summary of observations made on serrated flow behavior in alloy 625.

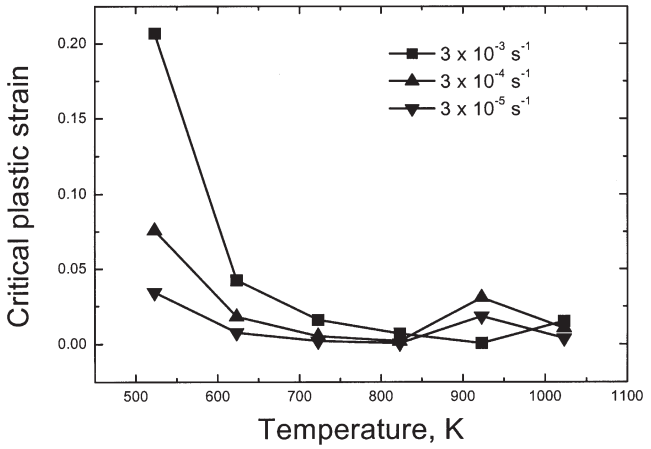

Fig. 5—Plot of critical strain for the onset of serrations *vs* strain rate.

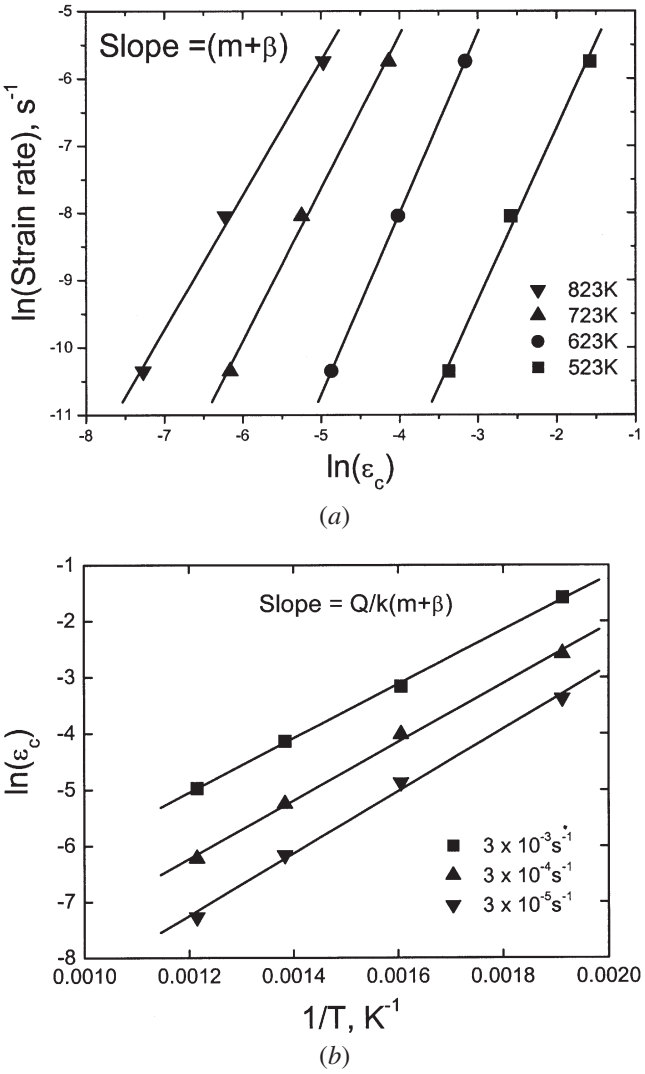

Fig. 6—Activation energy determination as per method: (*a*) plot of critical strain *vs* strain rate and (*b*) plot of critical strain *vs* 1/*T*.

Table I. ($m + \beta$) and Q Values (in kJ/mol) Obtained by Methods 1 through 3

	T: ($m+\beta$)			
$\dot{\varepsilon}$	523 K (2.3)	623 K (2.7)	723 K (2.3)	823 K (2.0)
Method 1:				
3×10^{-3} s^{-1}	92	109	92	81
3×10^{-4} s^{-1}	99	118	93	87
3×10^{-5} s^{-1}	106	125	106	93
Method 2: Q = 106 kJ/mol, 98 kJ/mol, 93 kJ/mol				
Method 3: At 3×10^{-3} s^{-1}; Q = 92 kJ/mol At 3×10^{-4} s^{-1}; Q = 94 kJ/mol At 3×10^{-5} s^{-1}; Q = 84 kJ/mol				

Fractographic studies conducted on samples tested at 1023 K at various strain rates indicate the occurrence of intergranular cracking at 3×10^{-5} s^{-1} (Figures 10(a) and (b)) and predominantly ductile fracture characterized by dimples at 3×10^{-3} s^{-1} (Figure 10(c)).

IV. DISCUSSION

A. *Tensile Behavior*

The tensile properties of the virgin material at room temperature obtained from the literature[25] are provided in Table III. The tensile properties of the present service-exposed alloy after resolution annealing at room temperature is also provided in the table for comparison. The temperature dependence of the tensile properties of alloy 625 in the service-exposed condition (exposed for 30,000 hours) has been investigated earlier by Raman *et al.*[26] These tests have been performed in the range of 300 to 973 K on samples taken from different portions of the cracker tube, which is exposed to service temperatures in the range of 773 to 973 K. For these conditions, the YS and UTS of the alloy have been reported to decrease with increase in test temperature. In the present study, the observed decrease in the YS of the alloy, in the solution-annealed condition, with increasing temperature is consistent with that reported by Raman *et al.* However, the temperature dependence of the YS showed peaks at 823, 723, and 923 K for 3×10^{-3} s^{-1}, 3×10^{-4} s^{-1}, and 3×10^{-5} s^{-1} strain rates, respec-

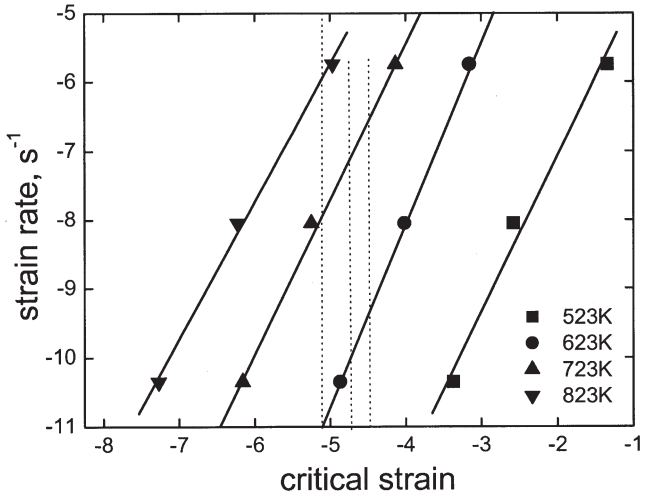

(*a*)

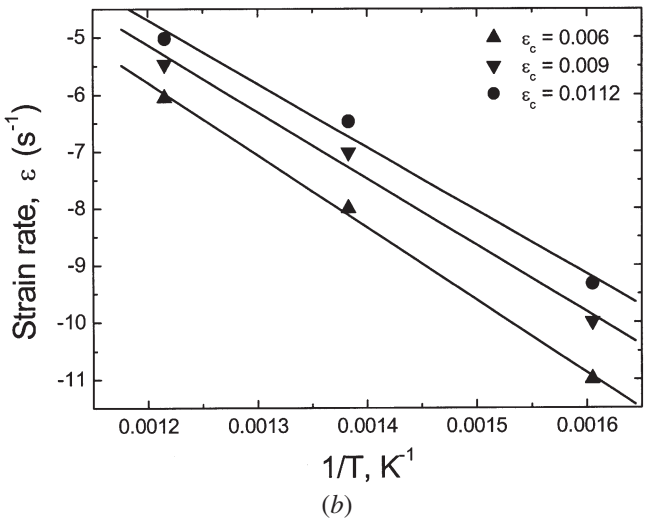

(*b*)

Fig. 7—Activation energy determination per method 2: (*a*) plot of strain rate *vs* ε_c and (*b*) plot of ln $\dot{\varepsilon}$ *vs* 1/*T* corresponding to critical strains represented by dotted vertical lines.

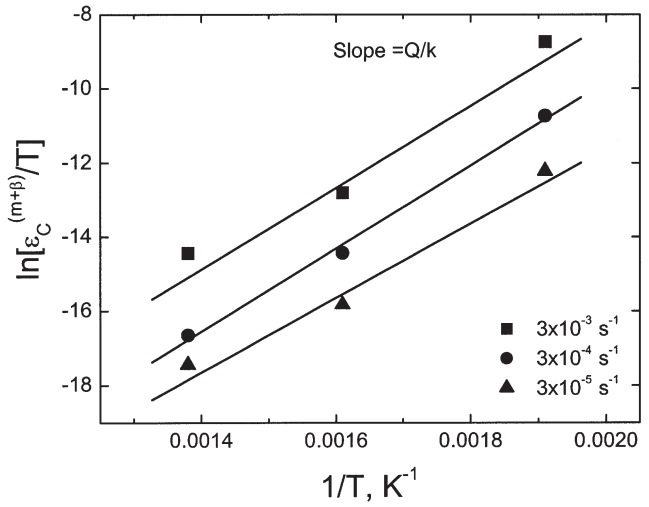

Fig. 8—Activation energy determination per method 3: plot of In $[\varepsilon^{(m+\beta)}/T]$ *vs* 1/*T*.

tively. The temperature range where the peaks have occurred in the YS, UTS, and work-hardening rate at different strain rates coincide with the range of temperatures in which serrated flow has been noticed (Figure 4).

Serrations in the load-elongation curve, which is one of the manifestations of DSA, results from interactions between solute atoms and mobile dislocations.[18] The sharp increase in work hardening with increasing temperature is observed at all the strain rates employed. Double peaks in the work-hardening *vs* temperature curve ((θ/E) *vs T,* Figure 9(d)) may be attributed to the operation of different mechanisms of DSA in the low- and high-temperature regimes. The occurrence of DSA in specific ranges and the associated high work-hardening rates and peaks/plateaus in the flow stress and UTS have been reported in several alloy systems by different investigators.[27–31] The increase in the work-hardening rate in the DSA regime is attributed to an increase in the rate of accumulation of dislocations.

A systematic shift of YS peaks toward higher temperatures with increasing strain rate has been reported in the NIMONIC* PE 16 superalloy by Rao *et al.*[32] However, such a systematic shift of the YS peaks with increasing temperature and strain rate has not been observed in this study of alloy 625. The behavior observed here is similar to that reported for alloy D9 by Venkadesan *et al.*[31] In alloy D9, the absence of such a systematic shift in the peak yield strength with temperature and strain rate has been reported to result from the multicomponent nature of the alloy, in which different solute species could contribute to DSA depending on temperature and strain rate. In alloy 625, in addition to the aforementioned, this can possibly be due to different precipitates forming at high temperatures during deformation. The various precipitates that form during static aging of the alloy at various temperature ranges are as follows. Precipitation of the metastable phase $\gamma''(Ni_3(Nb, Al, Ti))$, having an ordered bct DO_{22} structure,[1] occurs in the temperature range of 823 to 923 K.[2] Also, this metastable γ'' phase has a tendency to transform to the stable orthorhombic δ phase ($Ni_3(Nb, Mo)$) upon prolonged aging.[1–7,9,10] The δ phase has also been reported to form directly from the supersaturated solid solution on aging at temperatures higher than 1023 K.[8] Precipitation of $M_{23}C_6$, M_6C, and MC carbides will occur in the range of 1033 to 1253 K.[33] The primary MC carbides present in the undissolved state during solution annealing have been reported to decompose into $M_{23}C_6$ and M_6C on prolonged exposure at elevated temperatures.[33] Recent investigations have also revealed precipitation of $Ni_2(Cr, Mo)$ phase in alloy 625, which has a Pt_2Mo-type structure, by aging at temperatures below 873 K. The presence of this orthorhombic phase has been credited with causing low tensile and creep ductility and toughness in superalloys.[9,10,34–37]

The YS of the alloy increases at temperatures above 923 K when tested at a strain rate of $3 \times 10^{-3}\ s^{-1}$ (Figure 9(a)), possibly due to precipitation of γ''. The UTS falls off drastically above 923 and 873 K for $3 \times 10^{-4}\ s^{-1}$ and $3 \times 10^{-5}\ s^{-1}$, respectively (Figure 9(b)). Also, uniform elongation decreases sharply beyond 873 K for the slowest strain rate and beyond 923 K for the intermediate strain rate (Figure 9(d)).

Detailed fractographic studies indicated that intergranular cracking is more predominant at lower strain rates, which can

*NIMONIC is a trademark of Henry Wiggins & Company Ltd., Hereford, England.

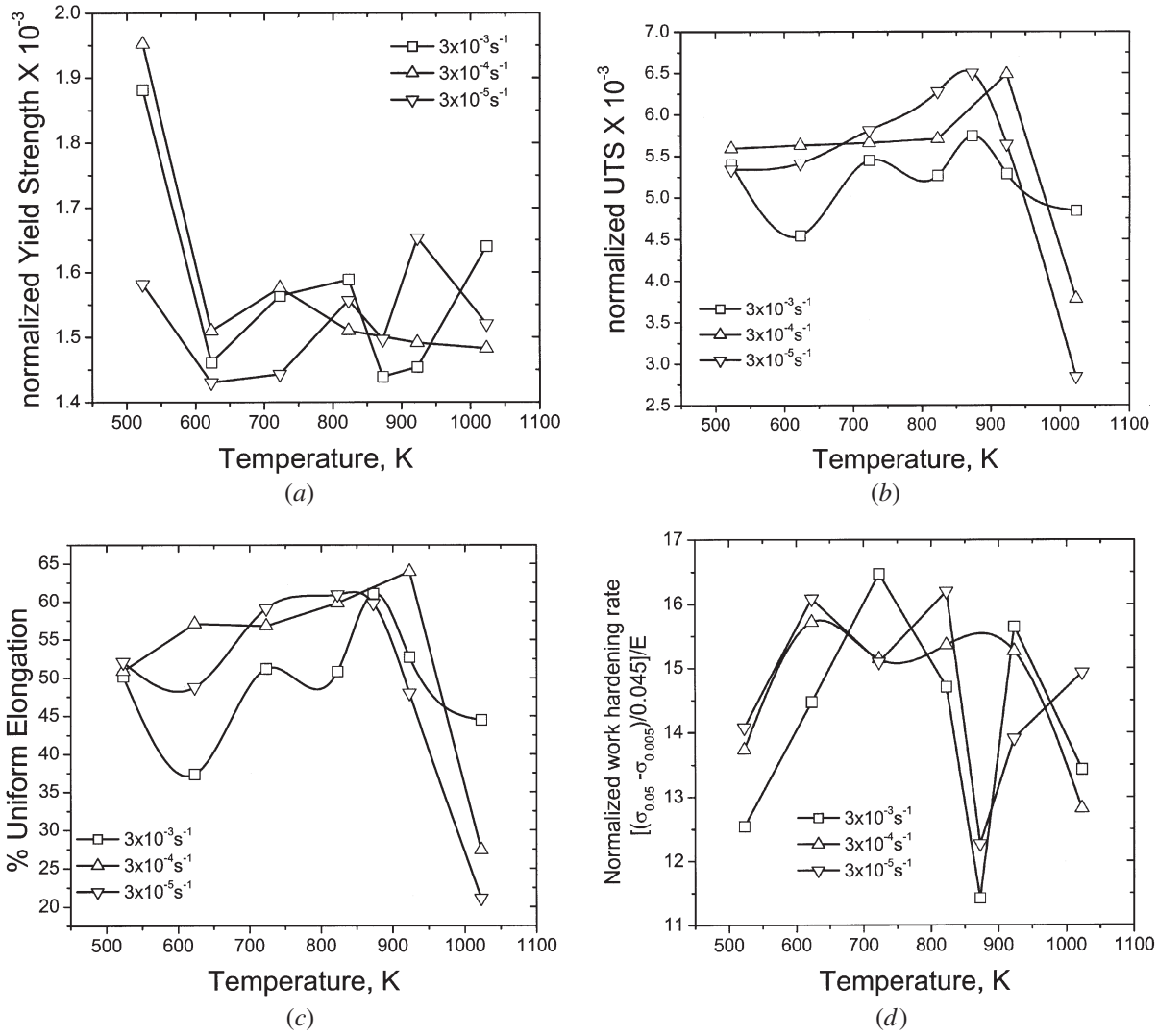

Fig. 9—(*a*) Effect of temperature and strain rate on 0.2 pct offset YS. (*b*) Effect of temperature and strain rate on UTS. (*c*) Variation of work hardening of alloy as a function of temperature and strain rate. (*d*) Effect of temperature and strain rate on uniform elongation.

Table II. Temperature Dependence of Young's Modulus of Elasticity[24]

T	Young's Modulus of Elasticity (GPa)
298	200
523	190
623	186
723	181.5
823	176.5
873	174
923	171
1023	165

be attributed to the precipitation of a network of grain-boundary carbides as well as δ phase along grain boundaries (Figures 10(a) and (b)), leading to a reduction in ductility at low strain rates compared to high strain rates. The reduction in uniform-elongation values above 873 K over specific strain rates is associated with the reduced ability of the material to work harden, which, in turn, leads to early necking. A positive strain-rate dependence of uniform elongation above 923 K is in agreement with the results previously reported for austenitic stainless steels,[31,37] in which a reduced tendency for grain-boundary sliding was considered to be the reason for such a dependence. The carbides that form in the present alloy are $M_{23}C_6$, M_6C, and MC and occur in the temperature range of 1033 to 1253 K. The $M_{23}C_6$ and MC carbides form primarily on the grain boundaries.[9,10] It is presumed that, during tension testing at high temperatures, precipitation can take place even at lower temperatures due to deformation-induced precipitation aided by enhanced diffusion of alloying elements constituting the precipitates. Decohesion of carbides on the grain boundaries and cracking of brittle phases like δ phase that form on the grain boundaries can increase the stress concentration on the grain boundaries, leading to intergranular fracture and a decrease in ductility at lower strain rates.

Further, the decrease in UTS beyond 923 and 873 K for strain rates of $3 \times 10^{-4}\,s^{-1}$ and $3 \times 10^{-5}\,s^{-1}$, respectively, could be attributed to the operation of a time-dependent restoration mechanism such as dynamic recovery, which could occur at lower temperatures for tests at lower strain rates. This behavior is similar to that observed in alloy D9.[31]

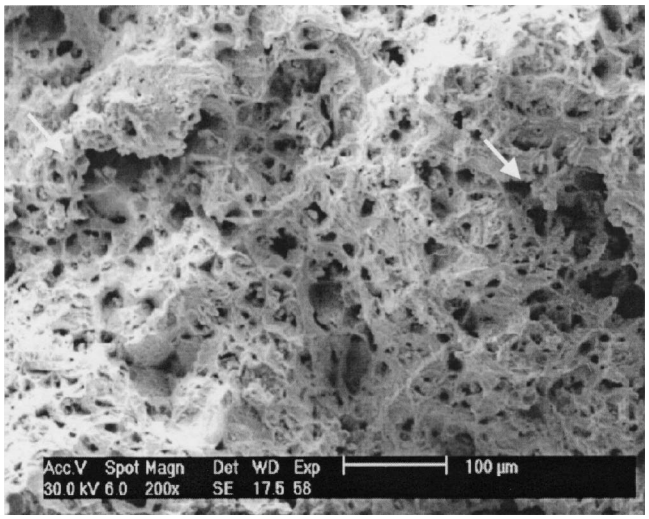

(*a*)

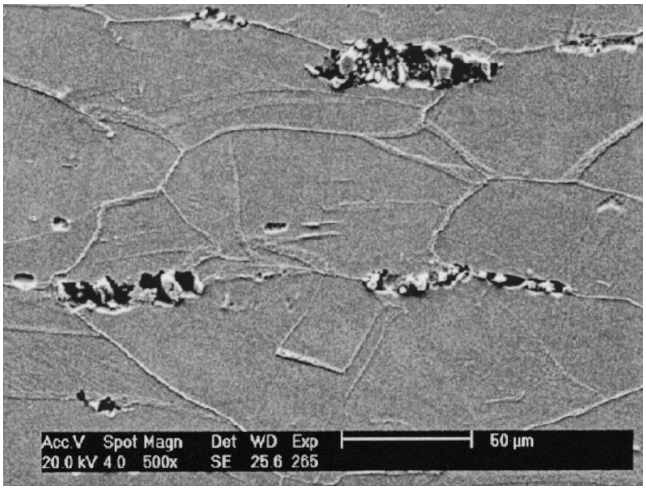

(*b*)

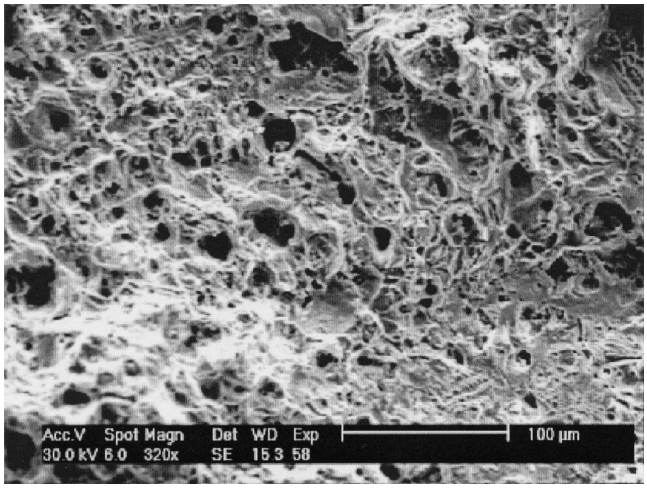

(*c*)

Fig. 10—(*a*) Fractograph of sample tested at 1023 K and 3×10^{-5} s^{-1} showing intergranular cracking (marked with arrows). (*b*) Micrograph of sample tested at 1023 K and 3×10^{-5} s^{-1} showing intergranular cracking. (*c*) Fractograph of sample tested at 1023 K and 3×10^{-3} s^{-1} showing ductile fracture.

Table III. Tensile Properties at Room Temperature of Virgin Alloy 625, the Service-Exposed Alloy (SE), and the SE Alloy That Was Solution Annealed (RSA)[9,25]

Product Form	Annealing Condition	Grain Size (μm)	YS (N/mm^2)	Pct Elongation
Virgin tube	1433 K/30 min/ quench	70	351	59
SE alloy (SE)	60,000 h aged/ 873 K	70	1013	5.8
RSA alloy (RSA)	1423 K/30 min/ quench	70	375	60.8

It is clear from Figure 9(c) that the samples tested at low strain rates (3×10^{-4} s^{-1} and 3×10^{-5} s^{-1}) exhibit pronounced uniform-elongation maxima at 923 and 873 K, respectively. There is a sharp decrease in the uniform elongation beyond 873 K at the lowest strain rate and beyond 923 K at the intermediate strain rate. It should be noted that the flow curves revealed type-C serrations at $T \geq 823$ K, for the lowest and intermediate strain rates, and at $T \geq 873$ K for the fastest strain rate. Below these temperatures, type-(A + B) serrations were observed (Figure 4). These results appear to indicate that the ductility maxima occurring at 873 K/3 $\times$ 10^{-5} s^{-1} and at 923 K/3 $\times$ 10^{-4} s^{-1} are associated with the onset of type-C serrations. This observation is contradictory to those reported by Koch and Troiano[39] and Barnby.[27] On the other hand, De Almeida and Monterio[40] reported that type-316 austenitic stainless steel tends to maintain a fairly high level of ductility in the DSA regime. Similarly, Rao *et al.* also observed ductility maxima in NIMONIC alloy PE 16 under conditions promoting type-C serrations.[32]

B. *Activation Energy for Serrated Flow*

Evaluation of activation energy is important to understand the mechanism of DSA. Generally, the values of activation energy depend on the method employed to evaluate them. It has been argued by Qian and Reed-Hill[19] that determination of Q from the ln ε_c *vs* 1/T plot involves assumptions about how ε_c varies as a function of mobile dislocation density and vacancy

concentration. They further point out that these assumptions are needed because the method uses data obtained over a range of strain rates and temperatures and that the procedure of assuming a constant $(m + \beta)$ value over the entire range is questionable. The intercept method, namely, method 2, as outlined in the introduction and shown in Figure 7, has been suggested as a better method. From the activation energies listed in Table I, an important observation to note is that the Q values determined from different methods are almost identical.

The activation energy for the onset of serrated yielding has been taken as the solute migration energy in Eq. [1]. The chemical composition of alloy 625 shows that the major substitutional alloying elements are Cr, Mo, Fe, and Nb. Since Cr and Fe are similar in atomic size to Ni,[21] the possible solute for the Cottrell type of locking may be Mo or Nb. Since Nb is known to be a slow-diffusing solute in Ni,[41] the possible solute responsible for DSA is Mo atoms. The activation energy for diffusion of Mo in Ni has been reported as 289 kJ/mol.[41] The activation energy may be composed of the vacancy-formation energy (Q_f) and the solute-migration energy (Q_m). The measured value of Q_f in Ni is 173 kJ/mol.[42] Therefore, the solute-migration energy of Mo in Ni can be estimated as 116 kJ/mol. The activation energy for the onset of serrated yielding in this alloy is found to be 98 kJ/mol, which agrees well with the previous assumption. This value is in agreement with the Q value (105 kJ/mol) for Mo migration in a Ni matrix in alloy 625, as reported by Kim and Chaturvedi.[21] Thus, we conclude that the substitutional solute Mo is responsible for the serrated flow in the low-temperature (<823 K) regime. This view is further corroborated by the observed $(m + \beta)$ values that lie between 2 and 3, indicating a substitutional diffusion-controlled mechanism of DSA (Table I). Generally, in DSA involving substitutional solutes, values of $(m + \beta)$ between 2 and 3 have been reported, whereas for DSA due to interstitial solutes, $(m + \beta)$ is usually closer to unity.[18]

The value of ε_c is dependent on both strain rate and temperature. At low and intermediate temperatures and at high strain rates (*i.e.,* for type A or B), ε_c increases with increasing $\dot{\varepsilon}$ and decreasing T. This is referred to as the normal PLE. On the other hand, at high temperatures and low strain rates (*i.e.,* for type C), ε_c increases with increasing T and decreasing $\dot{\varepsilon}$ (inverse PLE). Whereas the understanding of type-C unlocking serrations (inverse PLE) has not been very clear, most of the theoretical models based on DSA have been successful in explaining the normal PLE. It is believed that in the inverse PLE region, the diffusion rates are high enough for dislocations to be aged from the start of deformation, and type-C serrations appear to be due to breakaway of the aged dislocations.[43] It has been suggested[44] that unlocking serrations are connected with precipitation before and during the test. Hayes[45] and Hayes and Hayes[46] carried out systematic investigations in AISI 1020, 2.25 Cr-1Mo, alloy 718, and alloy 600 to relate the strain for disappearance of serrations with $\dot{\varepsilon}$ and T. They have shown that the disappearance of serrations from the flow curve occurs in the high-temperature regime by either a progressively longer strain to the onset of serrations (a critical-strain-delay mechanism) or by a progressively smaller strain to the disappearance of serrations (disappearance off the end of the flow curve). In the former case, carbon diffusing down the dislocation line to a precipitate sink is suggested as the mechanism; however, in the latter case, carbon reacting with a carbide-forming species on the dislocation line is responsible for the disappearance of serrations. Thus, the important conclusion from their studies is that the disappearance is generally related to a precipitation mechanism, and the disappearance of serrated flow would occur when a balance is reached between the growth of carbon atmosphere and its depletion due to reaction between substitutional (carbide-forming) atoms in the atmosphere. In this context, it has been suggested that the occurrence of type-C serrations could be regarded as a precursor to the precipitation and disappearance of serrations.[47]

The type-C serrations that occur at 823 K at the lowest strain rate (Figure 3) and at 873 and 923 K for the intermediate and highest strain rates, respectively (Figure 4), are discontinuous. This may be attributed to a solute-concentration fluctuation occurring in the matrix due to the mobility of the solutes and their interactions with the mobile dislocations. The solute concentration builds up by a diffusion process around the moving dislocations. If the solute concentration built around the dislocation is insufficient to lock up the dislocation, it may not lead to the formation of a serration. The solute concentration may not build up due to many reasons. Solutes may be involved in precipitation and may not be available for dislocation-solute interaction, or the time available for the concentration buildup may not be sufficient due to the application of a high strain rate. The correlations between the availability of diffusing species responsible for DSA, the formation of precipitates, and the disappearance of serrations have been reported earlier in several alloy systems by Hayes[45] and Hayes and Hayes.[46] It is presumed that in this alloy, the kinetics of precipitate formation ($(Ni_2(Cr, Mo)$, γ'', and carbides), which involves diffusion of elements such as Mo, Ti, and Nb, would have influenced the serration formation in the temperature range of 823 to 923 K.

It must be pointed out that the type-C serrations occurring in this alloy at high temperatures could have formed due to the following two reasons: (1) DSA effects resulting from the unlocking of dislocations from the atmospheres of substitutional solutes, as mentioned earlier, or (2) due to repeated shearing of the γ'' precipitates and $Ni_2(Cr, Mo)$ precipitates, formed during testing, by dislocations moving on the same slip plane. The mechanism of stress drop due to DSA is supported by Koul and Pickering[48] and also by the results reported in Fe-Ni-Cr alloys.[49] The stress drop due to shearing of γ' precipitates is advanced by Doi and Shimanuki[50] on the basis of their work on the UDIMET*

*UDIMET is a trademark of Special Metals Corporation, Huntington, WV.

alloy 520. Well-developed type-C serrations with a stress drop having a magnitude in the range 5 to 25 MPa were observed in this alloy on the stress-strain curve in the temperature range of 823 to 1023 K. Moreover, this is the temperature range in which precipitation of intermetallic phases, namely, $Ni_2(Cr, Mo)$ and γ'', occur upon aging the alloy.[2,9,10,37,51] It may be argued that these serrations could be a result of dynamic precipitation and subsequent shearing of fine $Ni_2(Cr, Mo)$ and γ'' in the temperature range of 823 to 1023 K during testing. Extensive transmission electron microscopy investigations on deformed samples are needed to reveal the exact mechanism for type-C serrations in INCONEL* alloy 625 in the temperature range of 823 to 1023 K.

*INCONEL is a trademark of INCO Alloys International, Huntington, WV.

V. CONCLUSIONS

High-temperature tension tests conducted on service-exposed alloy 625 after solution annealing led to the following conclusions

1. Dynamic strain aging was found to influence the tensile deformation of the alloy in the temperature range of 523 to 1023 K. Type-(A + B) serrations were observed at low temperatures (<823 K), whereas at higher temperatures, type-C serrations were seen.
2. The activation energy determined for serrated flow was found to be independent of the method employed, and the average Q value was obtained as 98 kJ/mol. Mo migration in the Ni matrix was proposed as the controlling mechanism for DSA in the low-temperature regime.
3. In the temperature and strain-rate regime where type-C serrations occurred, an inverse PLE was noticed. No Q values could be determined for this regime.
4. Other manifestations of DSA present were peaks/plateaus in the UTS and YS and work-hardening rate.
5. Reduction in ductility at $T > 923$ K with reduced strain rate was attributed to embrittlement of the grain boundary due to precipitation of carbides and δ phase.

ACKNOWLEDGMENTS

The authors acknowledge Dr. Baldev Raj, Director, MCRG, IGCAR, for many useful discussions and constant encouragement provided during the course of this investigation.

REFERENCES

1. E.E. Brown and D.R. Muzyka: in *The Superalloys II,* C.T. Sims and W.C. Hagel, eds., John Wiley, New York, NY, 1987, p. 165.
2. M. Sundararaman, Lalit Kumar, G.E. Prasad, P. Mukhopadhyay, and S. Banerjee: *Metall. Mater. Trans. A,* 1999, vol. 30A, p. 41.
3. H. Bohm, K. Ehlrich, and K.H. Krammer: *Metallurgy,* 1970, vol. 24, p. 643.
4. F. Garzarotli, A. Gerscha, and F.P. Francke: *Z. Metallkd.,* 1969, vol. 60, p. 643.
5. S. Floreen, G.E. Fuchs, and W.J. Yang: in *Superalloys 718, 625, 706 and Various Derivatives,* E.A. Loria, ed., TMS, Warrendale, PA, 1994, p. 13.
6. M. Sundararaman, P. Mukhopadhyay, and S. Banerjee: *Metall. Trans. A,* 1988, vol. 19A, pp. 453-65.
7. M. Sundararaman, P. Mukhopadhyay, and S. Banerjee: *Mater. Sci. Forum,* 1985, vol. 3, p. 273.
8. I. Kirman: *J. Iron Steel Inst.,* 1969, vol. 207, p. 1612.
9. Vani Shankar, K. Bhanu Sankara Rao, and S.L. Mannan: *J. Nucl. Mater.,* 2001, vol. 288, pp. 222-32.
10. Vani Shankar, M. Valsan, K. Bhanu Sankara Rao, and S.L. Mannan: *Scripta mater.,* 2001, vol. 44, pp. 2703-11.
11. L.Y. Popov and V.F. Sukharov: *Phys. Met. Metallogr.,* 1964, vol. 17 (3), p. 100.
12. R. Summerling and J. Nutting: *J. Iron Steel Inst.,* 1965, vol. 203, p. 398.
13. B.J. Brindley and P.J. Worthington: *Met. Rev.,* 1970, vol. 145, p. 101.
14. J.D. Baird: *Met. Rev.,* 1971, vol. 16, p. 1.
15. P. Rodriguez: *Encyclopedia of Materials Science and Engineering—Supplement:* R.W. Cahn, ed., Pergamon, 1988, vol. 1, pp. 504-08.
16. L.H. de Almeida and P.R.O. Emygdio: *Scripta Metall. Mater.,* 1994, vol. 31 (5), pp. 505-10.
17. P.G. McCormick: *Acta Metall.,* 1972, vol. 20, p. 351.
18. P. Rodriguez: *Bull. Mater. Sci.,* 1984, vol. 6, p. 653.
19. K.W. Qian and R.E. Reed-Hill: *Acta Metall.,* 1983, vol. 31, p. 87.
20. K. Mukherjee, C. Dantonio, R. Maciag, and G. Fischer: *J. Appl. Phys.,* 1968, vol. 39, p. 5434.
21. I.S. Kim and M. Chaturvedi: *Trans. Jpn. Inst. Met.,* 1987, vol. 28 (3), pp. 205-12.
22. E. Pink and A. Grinberg: *Acta Metall.,* 1982, vol. 30, p. 2153.
23. B. Russell: *Phil. Mag.,* 1963, vol. 8, p. 615.
24. *Aerospace Structural Metals Handbook,* Mechanical Properties Data Center, A DOD Materials information Center, Battelle Columbus Laboratories, Columbus, OH, 1982, vol 4, code 4117, p. 24.
25. *Superalloys 718, 625, 706 and Various Derivatives,* E.A. Loria, ed., TMS, Warrendale, PA, 1994.
26. V.V. Raman, G.E. Prasad, and P. Das Gupta: *Trans. Ind. Inst. Met.,* 1987, vol. 40, p. 113.
27. J.T. Barnby: *J. Iron Steel Inst.,* 1965, vol. 203, p. 392.
28. D.J. Michel, J. Moteff, and A.J. Lovell: *Acta Metall.,* 1973, vol. 21, p. 1269.
29. V. Kutumba Rao, D.M.R. Taplin, and P. Rama Rao: *Metall. Trans. A,* 1975, vol. 6A, pp. 77-86.
30. S.L. Mannan and P. Rodriguez: *Trans. Ind. Inst. Met.,* 1983, vol. 36, p. 313.
31. S. Venkatesan, S. Venugopal, M. Vasudevan, and P.V. Sivaprasad: *Mater. Sci. Technol.,* 1993, vol. 9, pp. 1-7.
32. K. Bhanu Sankara Rao, V. Seetharaman, S.L. Mannan, and P. Rodriguez: *High Temp. Mater. Processes,* 1986, vol. 7 (1), pp. 63-81.
33. D.R. Muzyka: in *The Superalloys 718,* C.T. Sims and W.C. Hagel, eds., Wiley, New York, NY, 1972, p. 113.
34. H.W. Tawancy, R.B. Herchenrocder, and A.J. Asphanani: *J. Met.,* 1983, vol. 35, p. 37.
35. H.W. Tawancy: *Metall. Trans. A,* 1980, vol. 11A, pp. 1784-85.
36. M. Kumar and V.K. Vasudevan: *Acta Mater.,* 1996, vol. 44, p. 1591.
37. Anish Kumar, Vani Shankar, T. Jayakumar, K. Bhanu Sankara Rao, and Baldev Raj: *Phil. Mag. A,* 2002, vol. 82 (13), p. 2529.
38. B. Ahlblom and R. Sandstrom: *Int. Metall. Rev.,* 1982, vol. 27, pp. 1-27.
39. C.C. Koch and A.R. Troiano: *Trans. ASM,* 1964, vol. 57, p. 519.
40. L.H. De Almeida and S.N. Monteiro: *2nd Int. Conf. on Mechanical Behavior of Materials,* ASM, Metals Park, OH, 1976, p. 1697.
41. R.A. Swalin: *Acta Metall.,* 1957, vol. 5, p. 443.
42. J. Friedel: *Dislocations,* Pergamon, Oxford, UK, 1964, p. 102.
43. W. Charnock: *Phil. Mag.,* 1969, vol. 20, p. 427.
44. A. Korbel, J. Zasadzinski, and Z. Sieklucka: *Acta Metall.,* 1976, vol. 24, p. 919.
45. R.W. Hayes: *Acta Metall.,* 1983, vol. 31, p. 365.
46. R.W. Hayes and W.C. Hayes: *Acta Metall.,* 1984, vol. 32, p. 259.
47. S. Venkadesan, C. Phaniraj, P.V. Sivaprasad, and P. Rodriguez: *Acta Metall.,* 1992, vol. 40, p. 569.
48. A.K. Koul and F.B. Pickering: *Scripta Metall.,* 1982, vol. 16, p. 119.
49. C.F. Jenkins and G.V. Smith: *Trans AIME,* 1969, vol. 245, p. 2149.
50. H. Doi and Y. Shimanuki: *Proc. 2nd Int. Conf. on Superalloys—Processing,* Champion, PA, 1972, Metals and Ceramics Information Centre, Columbus, OH, 1972, p. 0-1.
51. C. Thomas and P. Tait: *Int. J. Pressure Vessels Piping,* 1994, 59.